Amorphous Ni/Al nanoscale laminates as high-energy intermolecular reactive composites

Karthik Guda Vishnu, Mathew J. Cherukara, Hojin Kim, and Alejandro Strachan*
School of Materials Engineering and Birck Nanotechnology Center, Purdue University, West Lafayette, Indiana 47907, USA
(Received 29 September 2011; revised manuscript received 30 November 2011; published 15 May 2012)

We use molecular dynamics simulations to explore the potential use of amorphous metals in intermolecular reactive composites. Our simulations show that amorphous Ni/Al nanolaminates lead to an increase in temperature of up to 260 K over their crystalline counterparts; this increase corresponds to over 20% of the heat of fusion and can be explained in terms of the amorphization energy. The reactions are diffusion controlled and crystallization is observed in laminates with relatively long periods where high temperatures are experienced for sufficiently long times prior to intermixing; the effect of this process on the energetics and time involved in the reaction are characterized.

DOI: 10.1103/PhysRevB.85.184206 PACS number(s): 64.70.Nd, 61.43.Bn, 82.40.Ck

I. INTRODUCTION

Intermolecular reactive composites (IRCs) are high-energy density materials that sustain the propagation of exothermic reactions after thermal or mechanical initiation. They are an important class of active materials with defense and commercial applications, such as lead-free primers for explosives,[1,2] soldering,[3,4] and heat sources for medical applications. From a fundamental science standpoint, these nanostructured materials are extremely interesting as the initiation and propagation of reactions involve a complex set of coupled processes including condensed-phase chemistry, mass, and thermal transport in solid and liquid phases, and phase transformations; all occurring at high rates (reaction fronts with velocities of tens of m/s have been reported for Ni/Al systems) because of the large exothermicity of the reactions and small interdiffusion lengths.[5–7] Hence, molecular dynamics (MD) simulations are ideally suited to characterize the underlying atomic processes that govern the performance of these materials and the interplay between the above-mentioned processes. Recent experiments have captured the dynamical nature of the phase transformations using time-resolved synchrotron x-ray microdiffraction[6] and nanosecond *in situ* transmission electron microscopy (TEM)[5] in Ni/Al multilayer reactive foils. Both MD[8–12] and experimental investigations[6,13,14] revealed melting of the crystalline solids during the reaction of Ni/Al nanolaminates and Ni/Al nanoparticles, while evidence for solid-state reactions was observed in mechanically activated Ni/Al.[13] The process of melting absorbs a fraction of the energy generated during the chemical reactions (due to the heat of fusion) and consequently leads to a local drop in temperature degrading performance.[9,10,12] In this paper we explore the viability of amorphous materials for intermolecular reactive composites (aIRCs) which, with melting a second-order phase transition with no heat of fusion, we hypothesize will outperform their crystalline counterparts. We study the reaction mechanism in a model system consisting of alternating layers of amorphous Ni and amorphous Al and find that indeed these composites are more energetic than their crystalline counterparts and explain the increase in performance in terms of fundamental properties of the amorphous system. Ni/Al nanolaminates are chosen as our model material since they are among the most widely studied IRCs.[9,10,12,15–18] We point out that experimental realization of IRCs will likely require more complex alloys.[19]

II. COMPUTATIONAL DETAILS

We used LAMMPS[20,21] code to perform the MD simulations and the interaction between atoms is described by an embedded atom model recently developed by Purja and Mishin.[22] We model a single period in the laminate with Ni/Al interface normal along the z axis and impose periodic boundary conditions. We studied five systems of varying initial periodic length (from 12.54 to 37.63 nm) and an initial cross-sectional area of 8.1 $\times$ 8.1 nm. The initial Ni to Al ratio is set at 3.04 for all samples; Fig. 1(a) shows a snapshot of the initial configuration of the structure with periodic length 31.36 nm. The amorphous laminate samples are prepared from amorphous Ni and Al samples obtained by rapid heating and cooling using MD simulations. A MD time step of 1 fs is used to prepare the amorphous samples via heating and cooling. We initially heat crystalline samples up to 2300 K (above the melting temperature) in steps of 25 K running isothermal, isobaric MD simulations (NPT) for 100 ps at each temperature and cool down the samples to room temperature using the same rate also under NPT conditions. This leads to amorphous Ni and Al samples at room temperature from which we obtain the corresponding densities. In order to create Ni/Al nanolaminates we match the x and y cell dimensions of the Ni and Al 2300 K liquid samples setting the cell dimensions along z to match the room temperature density of the amorphous materials. The resulting structures are cooled down to 300 K with a rate of 100 K/50 ps using isochoric, isothermal MD (NVT ensemble). After creating the Ni and Al amorphous systems we bring them together into a single simulation cell and relax the system for an additional 65 ps under isobaric, isothermal conditions (NPT ensemble).

The nanolaminate samples are then rapidly heated to the desired initial reaction temperature (T_0) in 20 ps; this is followed by equilibration at T_0 for 10 ps also using NPT simulations. The chemical reactions of the equilibrated samples are then modeled with isobaric isoenthalpic MD simulations (NPH) at initial temperature T_0 and atmospheric pressure; this allows the system to heat up and change its volume due to the chemical reactions and has been used

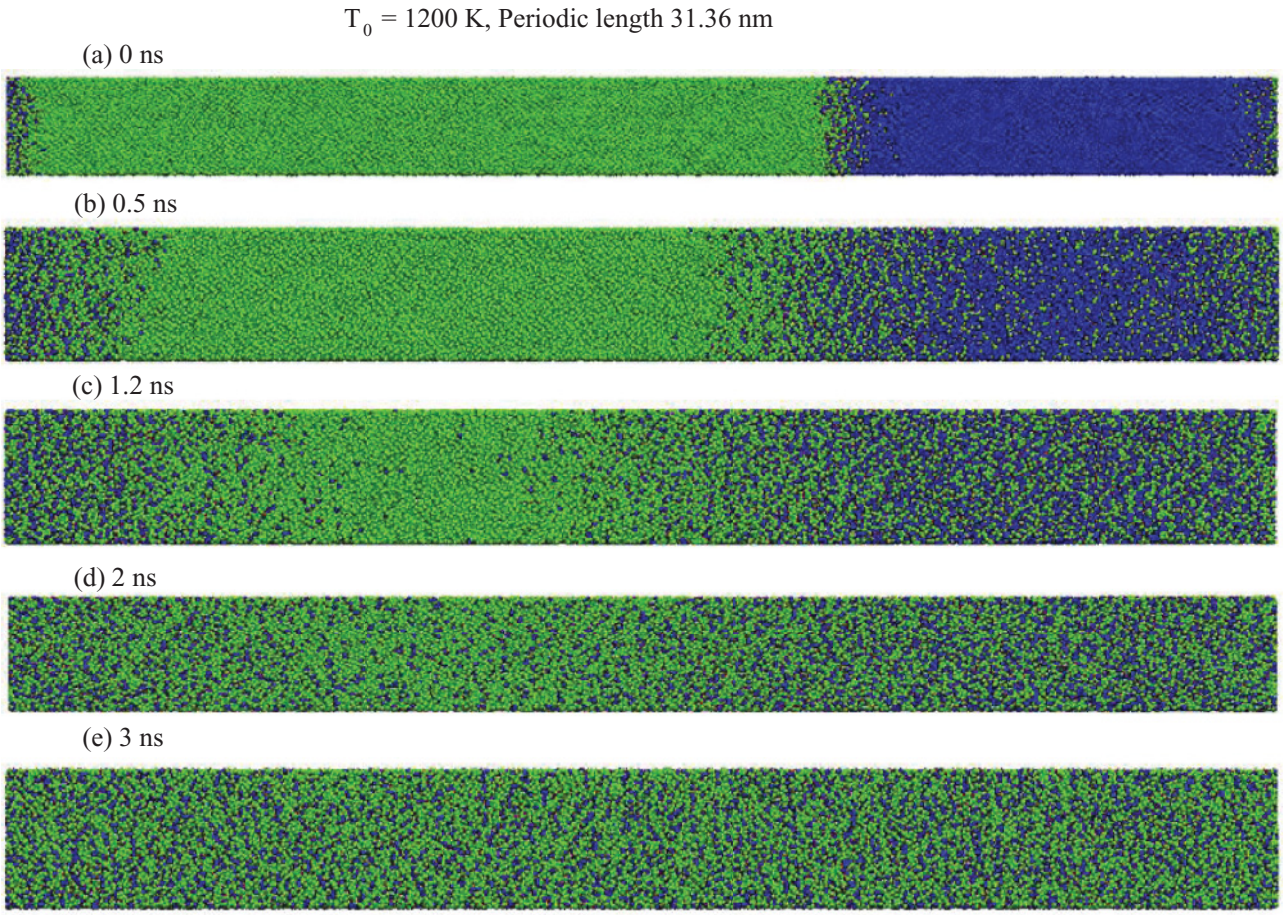

FIG. 1. (Color online) Snapshots of the amorphous intermolecular reactive composite at various times during the reaction, for the case $T_0 = 1200$ K and periodic length = 31.36 nm (Ni and Al are indicated by green (gray) and blue (black) colors, respectively).

before to study reactions in crystalline Ni/Al.[12] The time step used to integrate the equations of motion during chemical reaction is 0.5 femtoseconds with a velocity Verlet algorithm. The barostat relaxation constant is set at 1 ps. Every sample is simulated at three different reaction temperatures ($T_0 =$ 1200, 1100, and 900 K). Classical MD simulations ignore the electronic contribution to thermal transport and underestimate thermal conductivity. However, since chemical reactions are relatively slow (mass diffusivity is orders of magnitude lower than thermal diffusivity), temperature gradients remain small and the poor description of thermal transport has a negligible impact on our predictions.

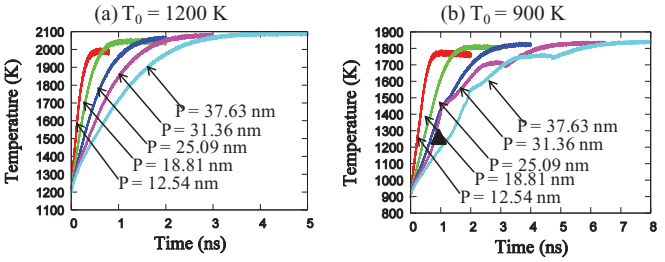

FIG. 2. (Color online) Temporal evolution of temperature during the reaction for all samples considered at (a) $T_0 = 1200$ K and (b) $T_0 =$ 900 K (triangle indicates the point at which Ni fully crystallizes in the sample with periodic length = 31.36 nm and $T_0 = 900$ K).

III. RESULTS AND DISCUSSION

Figures 1(a)–1(e) show snapshots of a sample with 31.36 nm periodic length reacting at initial temperature $T_0 =$

TABLE I. Asymptotic final temperature (T_{fin}, K) and τ (critical reaction time, ns) for all the cases studied.

Initial periodic length (P, nm)	Reaction temperature (T_0, K)	Asymstotic final temperature (T_{fin}, K)	Effective reaction time (τ, ns)
12.54	1200	1987.58	0.15
	1100	1908.09	0.19
	900	1760.20	0.31
18.81	1200	2040.46	0.29
	1100	1955.31	0.38
	900	1802.57	0.67
25.09	1200	2060.24	0.52
	1100	1978.51	0.65
	900	1820.64	1.11
31.36	1200	2076.98	0.74
	1100	1988.52	0.96
	900	1830.05	1.40
37.63	1200	2085.69	1.04
	1100	1998.31	1.31
	900	1836.91	1.92

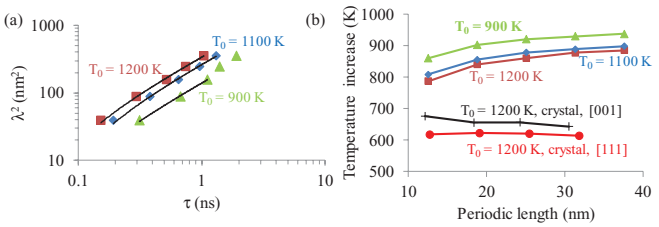

FIG. 3. (Color online) (a) Square of effective transport length (λ) versus critical reaction time (τ) in logarithmic scale for $T_0 = 1200$, 1100, and 900 K. (b) Temperature increase (K) versus initial periodic length ($P = 2\lambda$).

1200 K during the NPH simulations. Initially the reaction proceeds rapidly in the Al region [see Fig. 1(b)]. Simultaneously, reaction proceeds in the Ni region but at a slower speed and the overall kinetics slow down when the two fronts meet in the Ni region and disappear [Figs. 1(c)–1(e)]. Figure 2 shows the time evolution of temperature for various sample sizes at initial temperatures $T_0 = 1200$ and 900 K (the behavior for $T_0 = 1100$ K is very similar to that of 1200 K). For the two highest temperatures studied and shorter periods for $T_0 = 900$ K the temporal evolution shows a steep initial temperature increase that slows down as the reactions proceed to completion and the temperature reaches its asymptotic value (T_{fin}). This behavior can be described by the following equation:

$$T(t) = T_{\text{fin}} + (T_0 - T_{\text{fin}}) \times \exp(-t/\tau), \qquad (1)$$

where τ is the effective reaction time. T_{fin} is computed as the average temperature of the last 0.2 ns of every simulation and τ is obtained by fitting the temperature-time data of the MD simulations to Eq. (1). Table I summarizes the resulting reaction time scales for all cases studied.

As expected, τ increases with increasing periodic length at a fixed T_0 and with decreasing T_0 for a specific periodic length. Taking half of the initial periodic length of each laminate as the effective transport length (λ) we explore the reaction kinetics analyzing the resulting relationship between effective transport length and effective reaction time [Fig. 3(a)]. Our MD simulations show a linear relationship between square of the transport length and reaction time (the exponents of the fits are 1.135 ± 0.02, 1.135 ± 0.01, and 1.09 ± 0.02 at 1200, 1100, and 900 K, respectively). This clearly shows that the reactions are diffusion controlled; similar exponents are found in crystalline IRCs indicating a similar mechanism. The resulting effective diffusion constants[23] are 3.33×10^{-8}, 2.52×10^{-8}, and 1.85×10^{-8} m^2/s at 1200, 1100, and 900 K, respectively. The diffusion constant of Ni in liquid Al at 1091 K lies in the range 0.491×10^{-8} to 0.643×10^{-8} m^2/s (Ref. 24), which compares well with the MD results. The fact that the overall chemistry is diffusion controlled and the relationship between nanostructure (period in this case) and reaction time scales are among the main results of this paper.

Figure 3(b) shows the resulting temperature increase ($T_{\text{fin}} - T_0$) due to the reactions as a function of laminate period for the aIRCs and for corresponding crystalline ones, with (001) and (111) interfaces. The amorphous laminates exhibit

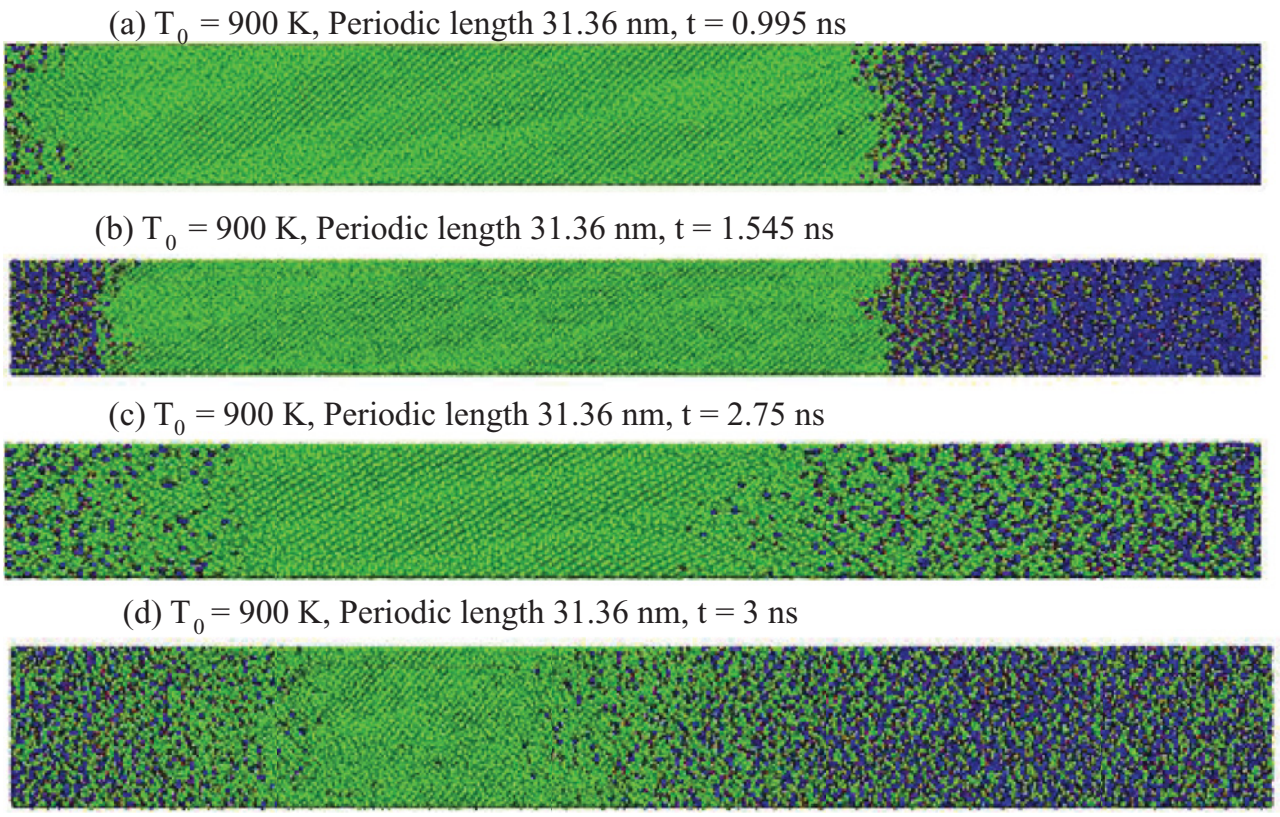

FIG. 4. (Color online) Snapshot showing crystallization of Ni for case $T_0 = 900$ K and initial periodic length = 31.36 nm: (a) $t = 0.995$ ns, (b) $t = 1.545$ ns, (c) 2.75 ns, and (d) 3 ns (Ni and Al are indicated by green (gray) and blue (black) colors, respectively).

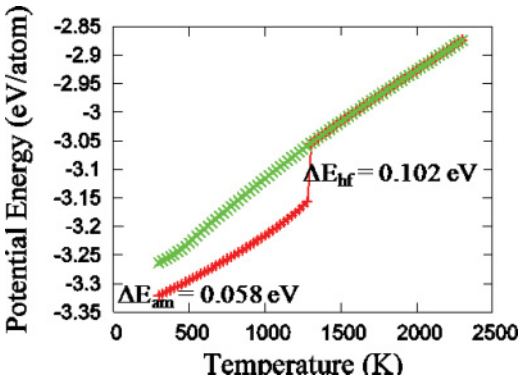

FIG. 5. (Color online) Potential energy (eV/atom) versus temperature (K) for pure Al.

greater exothermicity than their crystalline counterparts in all cases with a difference between 110 and 260 K for $T_0 = 1200$ K cases. The fact that the exothermicity increases with increasing periodic length can be attributed to the larger role played by the partially reacted interfaces at smaller periods. Simulations of the crystalline laminates have been carried out using the same approach used for the amorphous cases as explained above. The heat of fusion (ΔE_{hf}) for pure Ni and Al are determined to be 0.186 and 0.102 eV/atom, respectively, for the interatomic potential used (see Figs. 5 and 6). The maximum difference in temperature increase between the amorphous and crystalline samples (∼260 K) corresponds to 20% of the heat of fusion of the composite system. The amorphization energy (ΔE_{am}), defined as the difference in internal energy between the crystalline system and amorphous systems at 300 K, is perhaps a more relevant measure of the expected enhancement. We calculate ΔE_{am} to be 0.089 eV/atom for Ni and 0.058 eV/atom for Al and the increase in temperature corresponds to 42% of the ΔE_{am} of the system. This is very close to the idealized behavior one would obtain if all products and reagents were harmonic solids; under these conditions the difference in energy released would be spent to increase the potential and kinetic energy of the system in equal amounts due to the principle of equipartition of energy. The difference in exothermicity between amorphous and crystalline laminates decreases with decreasing period due to the increasingly important role of the Ni/Al interfaces.

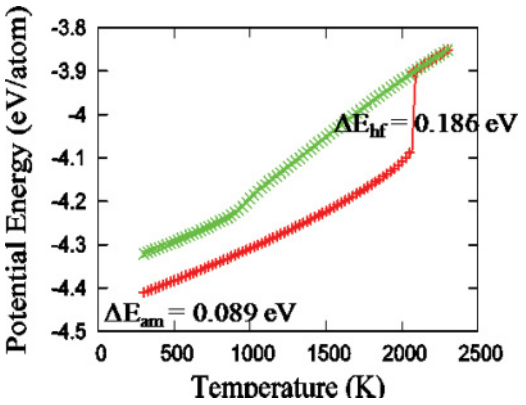

FIG. 6. (Color online) Potential energy (eV/atom) versus temperature (K) for pure Ni.

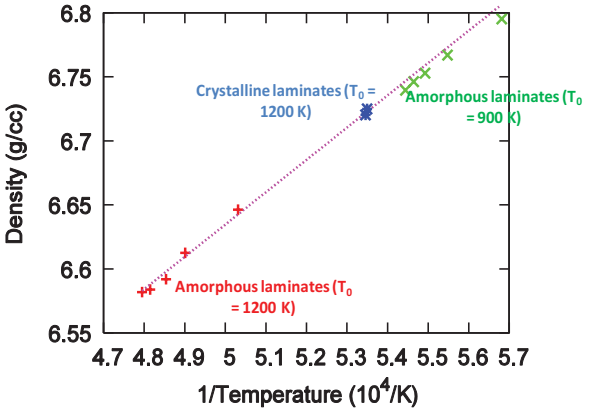

FIG. 7. (Color online) Density versus inverse temperature for final products of the reaction starting from crystalline and amorphous laminates.

We now focus on the reactions at $T_0 = 900$ K for the amorphous laminates with larger periodicities that exhibit a temperature evolution in marked contrast with all the other simulations (see Fig. 2). Both of these cases exhibit complex reaction mechanisms that were not observed in reactive composites previously. In all our simulations the Al region reacts faster and the amorphous Ni slabs remain at a high temperature and only partially reacted for a longer period of time. We find that for the lower temperature studied in this work and long-period laminates, amorphous Ni remains unreacted and at a high temperature for enough time for the metastable amorphous structure to crystallize. Figure 4(a) shows that the entire unreacted Ni region becomes crystalline 0.995 ns after the reaction is initiated. As shown in detail in the Appendix, we observe a crystalline nucleus at time 0.72 ns and a crystallization front propagating with a velocity of ∼60 nm/ns along the laminate direction. A similar phenomenon, denoted *explosive crystallization,* has been observed in a variety of thin films and multilayers, including Rh/Si multilayers,[25] Sb,[26] and Si[27,28] films. Following this crystallization event the chemical reactions proceed into crystalline Ni, as shown in Figs. 4(b)–4(d).

Not surprisingly, crystallization during the chemical reaction does not affect the overall energetics of the aIRC [Fig. 3(b)]. Since the reactions occur under isoenthalpic conditions the increase in average kinetic energy (and consequently temperature) during the reaction can be obtained as $\langle K\rangle_{\mathrm{aIRC}} - \langle K\rangle_{\mathrm{liq}} = \langle PE\rangle_{\mathrm{aIRC}} - \langle PE\rangle_{\mathrm{liq}} + P_0(\langle V\rangle_{\mathrm{aIRC}} - \langle V\rangle_{\mathrm{liq}})$, where K, PE, V, and P_0 are kinetic and potential energies, volume, and ambient pressure, respectively; brackets indicate time average and the subscripts indicate the initial aIRC and the final NiAl liquid. Thus, as long as the reactions proceed to completion and the resulting liquid is in equilibrium, the exothermicity is a state variable, independent of the path taken by the system. More interesting is the fact that partial crystallization does not slow down the overall reaction kinetics [see Fig. 3(a)]. Actually, the heat released during crystallization leads to a speed up of the reaction rates: see Fig. 2(b) where the triangle indicates the end of the crystallization process. We note that in macroscopic samples where chemical reactions occur in a spatially heterogeneous way, heat dissipation and internal mechanical work can cause

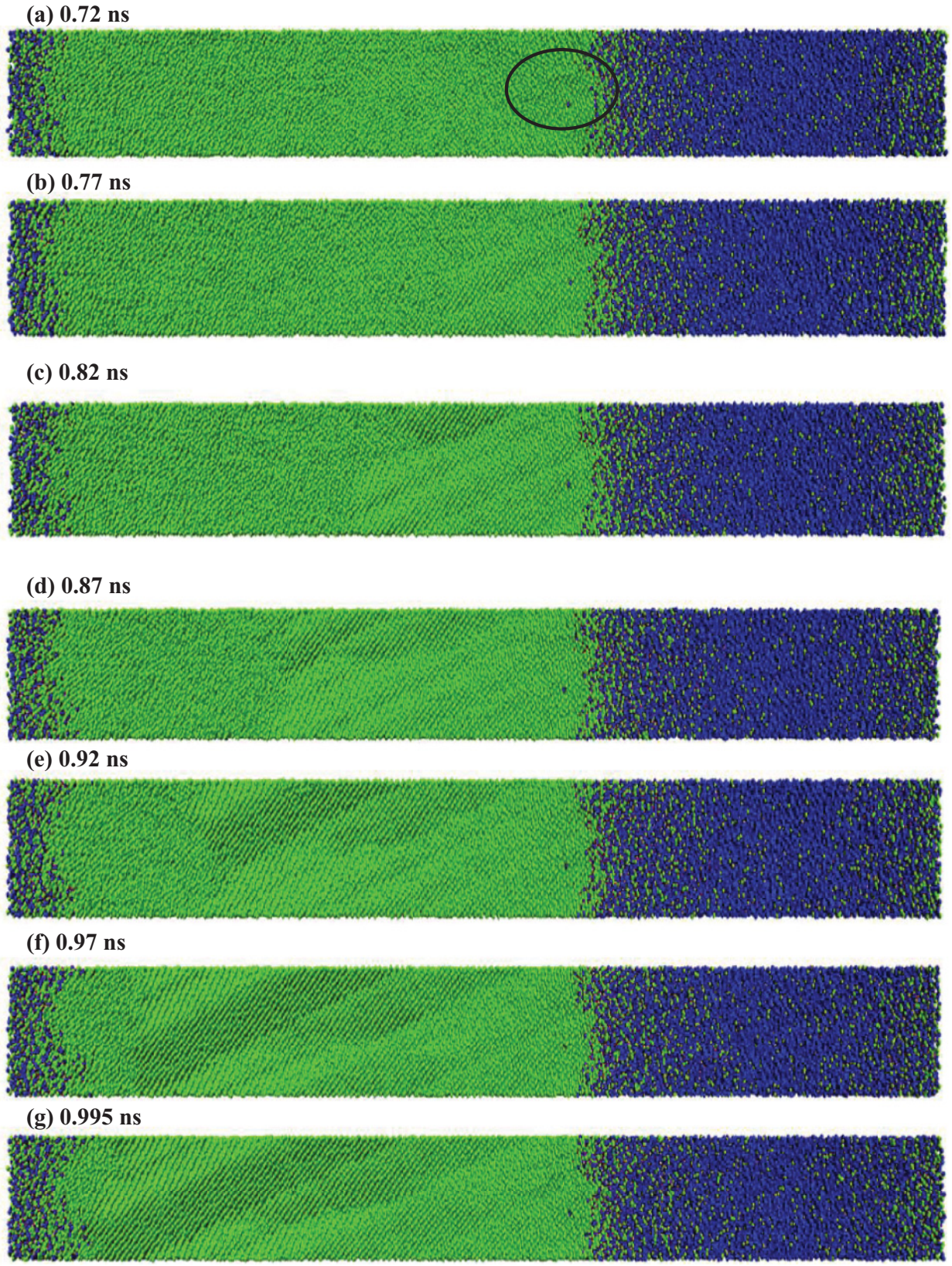

FIG. 8. (Color online) Snapshots showing (a) initial nucleation of crystalline Ni (highlighted by the black oval) in periodic length 31.36 nm and $T_0 = 900$ K nanolaminate and subsequent propagation [(b)–(f)] up to full crystallization of Ni (g) which occurs around 0.995 ns (Ni and Al are indicated by green (gray) and blue (black) colors, respectively).

crystallization to affect exothermicities and reaction time scales.

IV. SUMMARY AND CONCLUSIONS

In summary, our simulations show that amorphous metallic alloys are attractive alternatives to crystalline materials for intermolecular reactive composites and provides an unexplored avenue for optimization of this important class of materials. While the model Ni/Al system we studied would likely not be realizable in practice, a large number of metallic glasses exist today,[19] many of which could be used for IRC applications. Our simulations also show that partial crystallization due to the high temperatures during reaction does not degrade the performance of the composites. The theoretical results presented here show that the exploration of amorphous metals for energetic material applications could lead to new and improved formulations.

ACKNOWLEDGMENTS

This work was supported by the US Department of Energy Basic Energy Sciences (DoE-BES), DE-FG02-07ER46399 (Program Manager, J. Vetrano), and by the US Defense Threat Reduction Agency, HDTRA1-10-1-0119 (Program Manager, Suhithi Peiris). Computational resources of nanoHUB.org are gratefully acknowledged.

APPENDIX

1. Heat of fusion and amorphization energies

The heat of fusion and amorphization energies the Ni and Al used in this paper are computed from MD simulations of melting and rapid cooling. Figures 5 and 6 show potential energy (eV/atom) (running average over 40 ps) as a function of temperature during heating and cooling of pure Ni (48668 atoms) and pure Al (16000 atoms) at rates of 0.25 K/ps. Pure Ni melts at 2075 K and pure Al melts at 1275 K. Heat of fusion ($\Delta E_{\rm hf}$) and heat of amorphization ($\Delta E_{\rm am}$) are obtained from the potential energies as

$$\Delta E_{\rm hf}^{\rm Ni} = E_{\rm pot}^{\text{liquid Ni}}(T = 2075\ {\rm K}) - E_{\rm pot}^{\text{Xtal Ni}}(T = 2050\ {\rm K}),$$

$$\Delta E_{\rm hf}^{\rm Al} = E_{\rm pot}^{\text{liquid Al}}(T = 1275\ {\rm K}) - E_{\rm pot}^{\text{Xtal Al}}(T = 1250\ {\rm K}),$$

$$\Delta E_{\rm am}^{\rm Ni/Al} = E_{\rm pot}^{\text{amorphous Ni/Al}}(T = 300\ {\rm K}) - E_{\rm pot}^{\text{Xtal Ni/Al}}(T = 300\ {\rm K}).$$

2. Equation of state for products

Figure 7 shows the equation of state for the products after the reactions are completed. Density and inverse temperature of the final products show a linear relationship independent of the reaction temperature (T_0) and the nature of the nanolaminates. This shows that regardless of its initial conditions the reactive simulations lead to the same products.

3. Crystallization process and front speed

Figure 8 shows the initial crystallization event and propagation for a laminate with periodic length 31.36 nm and $T_0 =$ 900 K. An approximate value of the propagation velocity of the crystalline front can be obtained by visual inspection of the atomic snapshots. The initial crystallization occurs around time $t = 0.72$ ns. The crystalline region grows with time by propagating into the Ni region. The process has propagated roughly midway into the Ni region by time $t = 0.85$ ns [see Figs. 8(c) and 8(d)]. Crystallization reaches completion around time $t = 0.98$ ns between Figs. 8(f) and 8(g). The crystallization front travels approximately 15 nm in this time of 0.26 ns. Hence, we predict an approximate propagation velocity of ~60 nm/ns = 60 m/s for the crystallization front which can be compared to the typical experimental velocities for explosive crystallization of meters per second at lower temperatures.[29]

*strachan@purdue.edu

[1] J. J. Giles, Nature (London) **427**, 580 (2004).
[2] K. T. Higa, J. Propul. Power **23**, 722 (2007).
[3] A. J. Swiston Jr., E. Besnoin, A. Duckham, O. M. Knio, T. P. Weihs, and T. C. Hufnagel, Actamaterialia **53**, 3713 (2005).
[4] J. Wang, E. Besnoin, A. Duckham, S. J. Spey, M. E. Reiss, O. M. Knio, M. Powers, M. Whitener, and T. P. Weihs, Appl. Phys. Lett. **83**, 3987 (2003).
[5] J. S. Kim, T. LaGrange, B. W. Reed, M. L. Taheri, M. R. Armstrong, W. E. King, N. D. Browning, and G. H. Campbell, Science **321**, 1472 (2008).
[6] J. C. Trenkle, L. J. Koerner, M. W. Tate, S. M. Gruner, T. P. Weihs, and T. C. Hufnagel, Appl. Phys. Lett. **93**, 081903 (2008).
[7] D. S. Moore, S. F. Son, and B. W. Asay, Propellants, Explos. Pyrotech. **29**, 106 (2004).
[8] B. J. Henz, T. Hawa, and M. Zachariah, J. Appl. Phys. **105**, 124310 (2009).
[9] S. Zhao, T. C. Germann, and A. Strachan, Phys. Rev. B **76**, 014103 (2007).
[10] S. Zhao, T. C. Germann, and Alejandro Strachan, J. Chem. Phys. **125**, 164707 (2006).
[11] S. Zhao, T. C. Germann, and A. Strachan, Phys. Rev. B **76**, 104105 (2007).
[12] N. Scott Weingarten, W. D. Mattson, A. D. Yau, T. P. Weihs, and B. M. Rice, J. Appl. Phys. **107**, 093517 (2010).
[13] A. S. Mukasyan, J. D. E. White, D. Y. Kovalev, N. A. Kochetov, V. I. Ponomarev, and S. F. Son, Physica B **405**, 778 (2010).
[14] L. Thiers, A. S. Mukasyan, and A. Varma, Combust. Flame **131**, 198 (2002).
[15] E. G. Colgan, M. Nastasi, and J. W. Mayer, J. Appl. Phys. **58**, 4125 (1985).
[16] E. Ma, C. V. Thompson, L. A. Clevenger, and K. N. Tu, Appl. Phys. Lett. **57**, 1262 (1990).
[17] E. Ma, C. V. Thompson, and L. A. Clevenger, J. Appl. Phys. **69**, 2211 (1991).

[18]J. C. Crone, J. Knap, P. W. Chung, and B. M. Rice, Appl. Phys. Lett. **98**, 141910 (2011).
[19]W. L. Johnson, JOM **54**, 40 (2002).
[20]S. J. Plimpton, LAMMPS code, [http://lammps.sandia.gov].
[21]S. J. Plimpton, J. Comput. Phys. **117**, 1 (1995).
[22]G. P. Purja and Y. Mishin, Philos. Mag. **89**, 3245 (2009).
[23]A. Fick, Philos. Mag. **10**, 30 (1855).
[24]T. Ejima, T. Yamamura, N. Uchida, Y. Matsuzaki, and M. Nikaido, J. Jpn. Inst. Met. **44**, 316 (1980).
[25]J. A. Floro, J. Vac. Sci. Technol. A **4**, 631 (1986).
[26]C. C. Coffin and S. Johnston, Proc. R. Soc. London, Ser. A **146**, 564 (1934).
[27]G. Auvert, D. Bensahel, A. Georges, V. T. Nguyen, P. Henoc, F. Morin, and P. Coissard, Appl. Phys. Lett. **38**, 613 (1981); **39**, 724 (1981).
[28]R. A. Lemons and M. A. Bosch, Appl. Phys. Lett. **39**, 343 (1981).
[29]Wim van Saarloos and John D. Weeks, Phys. Rev. Lett. **51**, 1046 (1983).